Author Manuscript

Author Manuscript

Author Manuscript

Author Manuscript

HHS Public Access

Author manuscript

J Mol Biol. Author manuscript; available in PMC 2020 August 03.

Published in final edited form as:

J Mol Biol. 2011 March 04; 406(4): 620–630. doi:10.1016/j.jmb.2010.12.044.

Alternative Allosteric Mechanisms Can Regulate the Substrate and E2 in SUMO Conjugation

Ezgi Karaca[1], **Melda Tozluoğlu**[1], **Ruth Nussinov**[2,3,*], **Türkan Haliloğlu**[1,*]

[1]Polymer Research Center & Chemical Engineering Department, Bogazici University, Bebek-Istanbul 34342, Turkey

[2]Basic Science Program, SAIC-Frederick, Inc., Center for Cancer Research Nanobiology Program, NCI-Frederick, Frederick, MD 21702, USA

[3]Sackler Institute of Molecular Medicine, Department of Human Genetics and Molecular Medicine, Sackler School of Medicine, Tel Aviv University, Tel Aviv 69978, Israel

Abstract

Sumoylation is the covalent attachment of small ubiquitin-like modifier (SUMO) to a target protein. Similar to other ubiquitin-like pathways, three enzyme types are involved that act in succession: an activating enzyme (E1), a conjugating enzyme (E2), and a ligase (E3). To date, unlike other ubiquitin-like mechanisms, sumoylation of the target RanGAP1 ($Target^{RanGAP1}$) does not absolutely require the E3 of the system, RanBP2 ($E3^{RanBP2}$), since the presence of E2 ($E2^{Ubc9}$) is enough to sumoylate $Target^{RanGAP1}$. However, in the presence of E3, sumoylation is more efficient. To understand the role of the target specificity of $E3^{RanBP2}$ and $E2^{RanBP2}$, we carried out molecular dynamics simulations for the structure of $E2^{Ubc9}$–SUMO–$Target^{RanGAP1}$ with and without the $E3^{RanBP2}$ ligase. Analysis of the dynamics of $E2^{Ubc9}$–SUMO–$Target^{RanGAP1}$ in the absence and presence of $E3^{RanBP2}$ revealed that two different allosteric sites regulate the ligase activity: (i) in the presence of $E3^{RanBP2}$, the $E2^{Ubc9}$'s loop 2; (ii) in the absence of $E3^{RanBP2}$, the Leu65–Arg70 region of SUMO. These results provide a first insight into the question of how $E3^{RanBP2}$ can act as an intrinsic E3 for $E2^{Ubc9}$ and why, in its absence, the activity of $E2^{Ubc9}$–SUMO–$Target^{RanGAP1}$ could still be maintained, albeit at lower efficiency.

Keywords

Ubc9-RanGAP1; molecular dynamics; allostery; sumoylation cascade; E3-RanBP2

Introduction

Ubiquitin (Ub) and ubiquitin-like (Ubl) modifiers are proteins that mediate the post-transcriptional modification of specific targets. The small ubiquitin-like modifier (SUMO) family is a member of the Ub/Ubl superfamily. Four SUMO types were identified in

[*]*Corresponding authors*. R. Nussinov is to be contacted at NCI-Frederick, P.O. Box B, Building 469, Room 149, Frederick, MD 21702-1201, USA. T. Haliloğlu, Polymer Research Center, Bogazici University, Bebek 34342, Istanbul, Turkey. ruthnu@helix.nih.gov; turkan@prc.boun.edu.tr.

Supplementary materials related to this article can be found online at doi:10.1016/j.jmb.2010.12.044

Author Manuscript Author Manuscript Author Manuscript Author Manuscript

mammals: SUMO-1, −2, −3, and −4.[1–3] There are more than 100 SUMO targets for sumoylation, which are involved in, for example, subcellular localization, signal transduction, metabolic and transcriptional regulation, and modified enzyme activity.[4,5] Disturbing the sumoylation cascade can lead to neurological disorders such as Parkinson and Alzheimer diseases, loss of the genome integrity, developmental faults, and cancer.[2,6,7] SUMO conjugation involves a sequential cascade of three enzymes: SUMO activating enzyme (E1), SUMO-conjugating enzyme (E2), and SUMO ligase (E3). Initially, a protease cleaves the C-terminus of SUMO, exposing its Gly-Gly motif, which is next adenylated by an E1. The catalytic cysteine of the E1 attacks the adenylated C-terminus and forms a thioester bond, which is subsequently transferred to the E2 cysteine. In the last conjugation step, SUMO is transferred to an ε-amino group of a target lysine by the E3 enzyme.[8–14] It is currently believed that E3 is needed for two reasons: it can act as an adapter for SUMO and E2, thus imposing target specificity, and it enhances conjugation.[8,13,14] However, SUMO conjugation can also work well without an E3 for some targets that E2 recognizes and leads in *in vivo* sumoylation as, for example, in RanGAP1, p53, and IκBα targets.[3]

Although the general mechanism of sumoylation is known, the dynamic process on the atomic level and how signals are communicated in the structure are still open questions. For the last step of the conjugation (E2–E3–SUMO-1–Target), only one structure is available (PDB ID: 1Z5S)[15] (Fig. 1a). In this structure, Ubc9 is the E2 enzyme ($E2^{Ubc9}$), RanGAP1 is the target ($Target^{RanGAP1}$), RanBP2 ($E3^{RanBP2}$) is the E3 enzyme, and SUMO-1 (SUMO) is conjugated to the catalytic lysine of the target.

The $E2^{Ubc9}$ is highly conserved across species, and it is the only E2 enzyme known for SUMO family members.[3] It has the conserved superfold (UBC), which exists in all E2s of the Ub/Ubl superfamily. Among the E2s, there are some insertions into the UBC domain. In $E2^{Ubc9}$, there are only two amino acid insertions, Asp100 and Lys101.[16] These sites were suggested to have a role in target recognition.[16] The target interacting regions of $E2^{Ubc9}$ can be divided into two: (i) Lys74, Tyr87, Ser89, Thr91, Asp127, Pro128, and Ala 129, which form a catalytic pocket around the catalytic Cys93 of Ubc9 and the catalytic loop (Lys523–Glu526) of $Target^{RanGAP1}$[5,15,17–21] and (ii) the Ala131–Gln139 interface (third α-helix) of $E2^{Ubc9}$, which helps in forming a stable complex with $Target^{RanGAP1}$ (Fig. 1a). This binding site is unique among E2–Target pairs and is called “built-in E3,”[8] since $E2^{Ubc9}$ can function as an E2 enzyme even in the absence of an E3 by utilizing this additional binding site.[5,17,22]

The consensus SUMO interaction motif (SIM) on $Target^{RanGAP1}$ is ΨKX[D/E], where Ψ is an aliphatic or branched residue such as Ile, Val, or Leu; K is the lysine residue to which SUMO is conjugated; × is any residue; and D/E is aspartate or glutamate. The SUMO consensus motif is located between residues 523 and 526 (LKSE)[5,18–21] (Fig. 1a). The lysine residue, which attacks the thioester bond between SUMO and E2, is at position 524.[17] The two $Target^{RanGAP1}$ helices facing the “built-in E3” of Ubc9 lie between Thr511 and Leu522 and between Leu555 and Pro566[17] (Fig. 1a). $Target^{RanGAP1}$ without sumoylation is a cytosolic protein. It moves to the nuclear envelope during cell division and interacts with $E3^{RanBP2}$ after sumoylation.[17,23,24]

Author Manuscript Author Manuscript Author Manuscript Author Manuscript

SUMO ligase $E3^{RanBP2}$ is a large protein with 300 residues, but only a fragment was crystallized (Ser2629–Ser2693).[15] It has binding sites for $E2^{Ubc9}$, SUMO, and $Target^{RanGAP1}$ (Fig. 1a). The interaction surface between $E2^{Ubc9}$ and $E3^{RanBP2}$ is not a conserved E2–E3 interface, and the distance between this interface and the catalytic Cys of Ubc9 is more than 30 Å.[25] Several propositions have been made for the role of $E3^{RanBP2}$ in the sumoylation cascade: (i) Since $E3^{RanBP2}$ affects $Target^{RanGAP1}$ sumoylation *in vivo* but not *in vitro*, and $E2^{Ubc9}$ has an additional E2–Target interface, it was proposed that $Target^{RanGAP1}$ is sumoylated in order to form a stable complex with $E3^{RanBP2}$ at the nuclear pore[3,15,20,21,25,26,27]; (ii) $E3^{RanBP2}$ helps target sumoylation through an allosteric mechanism. Fixing the two reactants, $E2^{Ubc9}$ and SUMO, reduces the entropic cost of the system lowering the transition state barrier.[15,22] Related to this proposition, (iii) $E3^{RanBP2}$ optimally orients the structures, thus lowering the chance of nonproductive E2–SUMO conformations.[15,17,22,28] $E3^{RanBP2}$ was also proposed (iv) to promote the dissociation of the sumoylated target from the complex[29] and (v) to protect the sumoylated $Target^{RanGAP1}$ from isopeptidases.[27]

To clarify the catalytic role of $E3^{RanBP2}$ in the $E2^{Ubc9}$–$E3^{RanBP2}$–SUMO–$Target^{RanGAP1}$ system, we carried out molecular dynamics (MD) simulations. We modeled the step prior to catalysis, where the isopeptide bond between SUMO and $Target^{RanGAP1}$ is broken and a new thioester bond between SUMO and $E2^{Ubc9}$ is formed. The modeling is performed on the crystal structure of $E2^{Ubc9}$–$E3^{RanBP2}$–SUMO–$Target^{RanGAP1}$ (1Z5S) with and without $E3^{RanBP2}$ (Fig. 1b). In this work, we focused on the E2–Target dynamics in the absence and presence of $E3^{RanBP2}$, as the $E2^{Ubc9}$–SUMO complex dynamics were investigated earlier.[30] Comparative analyses between the MD simulations of the $E2^{Ubc9}$–$E3^{RanBP2}$–SUMO–$Target^{RanGAP1}$ and E2Ubc9–SUMO–$Target^{RanGAP1}$ complexes revealed that $E3^{RanBP2}$ provides slower exchange between the conformational ensembles for $E2^{Ubc9}$–SUMO–$Target^{RanGAP1}$, which may result in a decrease of the system's entropic cost as proposed by Reverter and Lima.[15] Furthermore, both in the absence and presence of the $E3^{RanBP2}$, the $E2^{Ubc9}$–$Target^{RanGAP1}$ interface residues are dynamically coupled, although to a lower extent in the absence of $E3^{RanBP2}$. As an explanation to the question of the role of $E3^{RanBP2}$ and how catalysis can be performed in its absence, we show that the system of $E2^{Ubc9}$–SUMO–$Target^{RanGAP1}$ could work through two distinct allosteric mechanisms: in the presence of $E3^{RanBP2}$, allostery is induced by $E2^{Ubc9}$, and in the absence of $E3^{RanBP2}$, by SUMO.

Results

$E3^{RanBP2}$ is an allosteric effector of the $E2^{Ubc9}$–SUMO–$Target^{RanGAP1}$ complex

The behavior of the $E2^{Ubc9}$–$E3^{RanBP2}$–SUMO–$Target^{RanGAP1}$ complex structure and its individual chains in the 48.5-ns MD simulation is first characterized by the root mean square deviation (RMSD) from the minimized X-ray structure. The overall structure is stable with low amplitude fluctuations. Since $E3^{RanBP2}$ is a fragment,[15] it presents high-amplitude RMSD fluctuations (Table 1). The RMSD of $E2^{Ubc9}$ suggests a relatively significant conformational change early in the simulations (at 16 ns) (Fig. 2a and b). Different from

Author Manuscript Author Manuscript Author Manuscript Author Manuscript

E3^{RanBP2} and E2^{Ubc9}, the RMSD of Target^{RanGAP1} and SUMO has a relatively stable profile (Table 1; Fig. 2a).

The observed RMSD jump of E2^{Ubc9} is mainly due to the conformational change of the loop between residues Lys30 and Thr35 (loop 2), where Asp33 has the highest mobility. Loop 2 is the most mobile part of E2^{Ubc9}, as also revealed by the mean-square fluctuations (MSF) of the residues (Table 2). Loop 2's mobility is coordinated via a hinge-like behavior of residues Phe24 and Glu42. Interestingly, the comparison of the E2^{Ubc9} fluctuations in the isolated state and in the E2^{Ubc9}–SUMO–Target^{RanGAP1} complex structure, with and without E3^{RanBP2}, indicates that loop 2 becomes more mobile when E2^{Ubc9} is bound to SUMO and Target^{RanGAP1} and strikingly gains further mobility upon E3^{RanBP2} binding (Table 2). On the other hand, E2^{Ubc9}'s two functional regions, mainly the catalytic cysteine (Cys93) and the built-in E3 (third α-helix), assume already rather restricted fluctuations upon SUMO and Target^{RanGAP1} binding (Table 2).

To identify the major sampled conformational states, the MD trajectory of E2^{Ubc9}–E3^{RanBP2}–SUMO–Target^{RanGAP1} is clustered by the RMSD between the conformations. When clustering at 2.5-Å RMSD, six clusters are generated (Fig. 3a). The RMSD jump of E2^{Ubc9} with loop 2's motion is reflected in the transition from the first to the second cluster. Analysis of the conformational ensemble of the first and second clusters reveals that there is a transition between the two dominant conformations of E2^{Ubc9}'s loop 2, a twisted and bent conformation and a relatively stable state also observed in the starting X-ray structure (PDB: 1Z5S; Fig. 2b). When plotting the clusters' evolution with respect to time, the simulation divides into six windows (Fig. 3a). For each time window and the entire simulation, the network of correlated fluctuations is calculated and illustrated as a correlation map. The most important coupled fluctuations that could be ascribed function are those observed between the E2^{Ubc9} binding sites of Target^{RanGAP1} and the E2 binding sites of Target^{RanGAP1} (Fig. 1a; Supplementary Fig. S2a). The fluctuations of E2^{Ubc9}'s loop 2 demonstrate strong correlations with the fluctuations of one of the explicit E2^{Ubc9} binding sites (Leu555–Pro566) of Target^{RanGAP1} for the whole simulation time. Further, during 77.5% (2–38 ns) of the simulation time, there is a correlation between the fluctuations of E2^{Ubc9}'s loop 2 and the SIM of Target^{RanGAP1} (Fig. 4). The latter correlation is persistently high in the first (2–15 ns) and third (19–24 ns) clusters and resides in 38.7% of the simulation time. Coupled to this, Asp33 of loop 2 is at its most mobile and flexible state during this time (Table 2). Along this time, Asp2665–Asp2673 on E3^{RanBP2}, which is a flexible linker connecting the two major helices of E3^{RanBP2}, displayed a unique mobile and slightly flexible behavior (Table 2). Taken together, these lead us to suggest that E3^{RanBP2} helps organize the network of coupled fluctuations of E2^{Ubc9} and thus of E2^{Ubc9}–Target^{RanGAP1} binding via E2^{Ubc9}'s loop 2.

Asp33 of E2^{Ubc9}'s loop 2 is 38.5 Å away from the catalytic lysine of Target^{RanGAP1}, yet its fluctuations are coupled to the catalytic SIM and E2^{Ubc9} binding site of Target^{RanGAP1}. Interestingly, Asp33, the most mobile and flexible residue of E2^{Ubc9}'s loop 2, has been strongly conserved in evolution.[31] Asp33's dynamics with respect to the E2^{Ubc9}–Target^{RanGAP1}interface, its conservation, and its position with respect to E3^{RanBP2} suggest

Author Manuscript Author Manuscript Author Manuscript Author Manuscript

that $E3^{RanBP2}$ is an allosteric effector of the $E2^{Ubc9}$–E3RanBP2–SUMO–$Target^{RanGAP1}$ complex.

An alternative sumoylation mechanism in the absence of $E3^{RanBP2}$

The dynamics of the $E2^{Ubc9}$–SUMO–$Target^{RanGAP1}$ complex structure is analyzed with respect to the same complex in the presence of $E3^{RanBP2}$. The RMSD values of the $E2^{Ubc9}$–SUMO–$Target^{RanGAP}$ complex structure and its individual chains with and without $E3^{RanBP2}$ revealed that the absence of $E3^{RanBP2}$ does not affect the average RMSD values, yet the range of the RMSD fluctuations differs. Further, removal of $E3^{RanBP2}$ results in higher RMSD values for $Target^{RanGAP1}$ and SUMO (Table 1; Fig. 2c). $E2^{Ubc9}$, however, does not reflect any RMSD jumps as observed in the presence of $E3^{RanBP2}$ (Fig. 2c). Thus, $E3^{RanBP2}$ affects the conformational space spanned both by the $E2^{Ubc9}$–SUMO–$Target^{RanGAP1}$ complex structure and its individual chains, which implies both conformational and configurational structural changes.

To compare the ensembles of conformations visited in $E2^{Ubc9}$–SUMO–$Target^{RanGAP1}$ with and without $E3^{RanBP2}$, we followed a step-by-step approach. First, we clustered the conformations from the simulations with and without $E3^{RanBP2}$, with an RMSD radius of 3 Å. The absence of a joint cluster of conformations suggests that $E2^{Ubc9}$–SUMO–$Target^{RanGAP1}$ with and without $E3^{RanBP2}$ do not display similar conformational states (Table 3). As discussed below, this is likely to be due to the orientation change of SUMO observed in the absence of $E3^{RanBP2}$ (Fig. 5a). The joined conformational ensembles are next searched for $E2^{Ubc9}$ conformations only (with 2.5-Å RMSD radius). This analysis showed that almost for the whole simulation time of the $E2^{Ubc9}$–SUMO–$Target^{RanGAP1}$ complex, the twisted/bent conformation of the $E2^{Ubc9}$ loop 2 is not visited (Table 3). For a finer search of the conformational states, individual clustering and clustering of the conformations from the trajectory without $E3^{RanBP2}$ are performed similarly as with $E3^{RanBP2}$, except using different RMSD radii (2.2 Å and 2.5 Å). The distribution of clusters (16 and 5 for 2.2 Å and 2.5 Å radius, respectively) along time showed that the transitions between different conformational states are more frequent without $E3^{RanBP2}$ (Fig. 3b). The 2.2-Å RMSD yielded a better distribution of the clusters' evolution as compared to 2.5 Å, more conveniently dividing the trajectory into time windows (Fig. 3b; Supplementary Fig. S1).

Unlike in the $E2^{Ubc9}$–$E3^{RanBP2}$–SUMO–$Target^{RanGAP1}$ simulation, only in 3 out of 16 clusters (26% of the simulation time; for the intervals of 4.5–5.5 ns, 15.5–17 ns, and 17–25 ns) coupled fluctuations are observed across the $E2^{Ubc9}$–$Target^{RanGAP1}$ interface (Supplementary Fig. S1). For the rest of the simulation, either no correlation or a nonuniformly distributed low correlation (74% of the simulation time) is observed (Supplementary Fig. S2b). Further, only in one of the three ensembles does the $E2^{Ubc9}$ loop 2 strongly correlate with the $E2^{Ubc9}$ binding and catalytic sites of $Target^{RanGAP1}$ (Fig. 5b). The residence time of this ensemble is over 21% of the simulation (17–25 ns). The mobility and flexibility of $E2^{Ubc9}$'s loop 2 is less restricted in this ensemble compared to the other clusters (Table 2). Thus, the correlation between the dynamical behavior of $E2^{Ubc9}$'s loop 2 and the strength of the cooperative fluctuations across the $E2^{Ubc9}$–$Target^{RanGAP1}$ interface

Author Manuscript Author Manuscript Author Manuscript Author Manuscript

observed for the E2Ubc9–E3^{RanBP2}–SUMO–Target^{RanGAP1} complex appears to also take place without E3^{RanBP2} (Table 2). This network of correlated fluctuations is coupled to the emergence of a new E2^{Ubc9}–SUMO interface when E3^{RanBP2} is not present. On the SUMO side, this interface is formed at the Leu65–Arg70 region and is mediated by the anchoring of SUMO's Gly68. This residue, which is fully conserved,[31] is 10.5 Å away from the closest E2^{Ubc9} residue in the crystal structure. The anchoring is indicated as SUMO's Gly68 approaches E2^{Ubc9}'s Lys49 and Gly50. Further, this new interface presents a correlated motion with part of the E2^{Ubc9} catalytic pocket (Asp127–Ala129). To this end, it is plausible to suggest that formation of this new interface shifts the E2^{Ubc9} conformational ensemble, similar to the E3^{RanBP2}-bound network of fluctuations in E2^{Ubc9}. The formation of the new interface thus provides a rationale for the orientational change in the quaternary structure of the E2^{Ubc9}–SUMO–Target^{RanGAP1} complex in the absence of E3^{RanBP2} (Fig. 5a).

Discussion

Here, we study the mechanism of the sumoylation cascade prior to the covalent attachment of SUMO to the substrate and the role of E3^{RanBP2}. Earlier, it was argued that E3^{RanBP2} helps to reduce the entropic cost of the system, lowering the conformational flexibility of SUMO and E2^{Ubc9}.[22] This can facilitate the passage through the transition state of the reaction, which implies that E3^{RanBP2} acts as a catalyst in the transfer of SUMO from E2 to the substrate. Based on the crystal structure of E2^{Ubc9}–E3^{RanBP2}–SUMO–Target^{RanGAP1}, we design two complexes, which serve as the basis for the dynamic simulations. The analysis of the time course of the conformations indeed suggests that the presence of E3^{RanBP2} restricts the transitions between the ensembles of accessible conformations and increases the cooperativity of E2^{Ubc9} with the E2^{Ubc9}–Target^{RanGAP1} interface. In the presence of E3^{RanBP2}, E2^{Ubc9}'s loop 2 demonstrates a highly mobile and flexible behavior. The fluctuations of loop 2 are allosterically coupled with the fluctuations of the SIM and E2^{Ubc9} binding sites on Target^{RanGAP1}, where Asp33 of this loop 2 of E2^{Ubc9} is 38.5 Å away from the catalytic lysine of Target^{RanGAP}. Interestingly, the E3^{RanBP2} free loop between Asp2665 and Asp2673, which is confined in the presence of E2^{Ubc9}, gains mobility, as loop 2 is coupled with the functional sites on Target^{RanGAP1}. These data suggest that E3^{RanBP2} is involved in the network of correlated fluctuations that couples the E2^{Ubc9} loop 2 with the catalytic sites of Target^{RanGAP1} and strengthens the binding between E2^{Ubc9} and Target^{RanGAP1}. This agrees with the proposition that E3^{RanBP2} could increase the affinity between Ubc9 and the target.[17]

E3^{RanBP2} may have a role in regulating catalytic efficiency.[15,22,28] Without E3^{RanBP2}, the exchange between conformational states is faster for the complex structure of E2^{Ubc9}–SUMO–Target^{RanGAP}, which might be an indication of a decrease in catalytic efficiency. The absence of a common conformational ensemble of E2^{Ubc9}–SUMO–Target^{RanGAP} with and without E3^{RanBP2} suggests that E3^{RanBP2} binding biases the conformational space sampled by the E2^{Ubc9}–SUMO–Target^{RanGAP} structure as well as the E2^{Ubc9}-only structure. The removal of E3^{RanBP2} significantly reduces the coupled fluctuations at the E2^{Ubc9}–Target^{RanGAP1} interface with a parallel decrease in the flexibility and mobility of E2^{Ubc9}'s loop 2 and in the correlation between E2^{Ubc9}'s loop 2 and the SIM and E2^{Ubc9} binding sites on Target^{RanGAP1}. Nevertheless, the emergence of the new interface between SUMO and

Author Manuscript Author Manuscript Author Manuscript Author Manuscript

E2^{Ubc9} with a quaternary change in the structure of the E2^{Ubc9}–SUMO–Target^{RanGAP1} complex regains the E3^{RanBP2}-bound network of fluctuations in E2^{Ubc9}. The new interface of SUMO (Leu65–Arg70) exhibits a correlated motion with one of the E2^{Ubc9} catalytic pocket loops concomitant with correlated fluctuations between E2^{Ubc9}'s loop 2 and the E2^{Ubc9}–Target^{RanGAP1} interface. Although E2^{Ubc9}–SUMO–Target^{RanGAP1} with and without E3^{RanBP2} do not have a joint conformational space, the structural readjustment with the new interface reassumes the network of correlated fluctuations that are expected to assist in the catalytic efficiency. This structural readjustment may explain why *in vitro* sumoylation of Target^{RanGAP1} is successful in the absence of E3^{RanBP2}.[3] To validate this proposed allosteric mechanisms, we carried out a second set of simulation for both complexes and observed that these corresponding mechanisms are persistently present in the absence and presence of E3^{RanBP2} for a significant period of the simulation time (for details, see Supplementary text, Supplementary Figs. S4–S6, and Supplementary Table S1).

To conclude, analysis of the dynamics of E2–Target in the absence and presence of E3^{RanBP2} and comparison with that of E2^{Ubc9}–E3^{RanBP2}–SUMO–Target^{RanGAP1} exhibits why Target^{RanGAP1} can be sumoylated in vitro without E3^{RanBP2} and also why E3RanBP2 affects sumoylation *in vivo*. In the latter case, E3^{RanBP2} allosterically preorganizes the structural environment for catalysis by restricting the conformational space. To this end, we propose two different allosteric sites that contribute to the ligase activity: (i) E2^{Ubc9}'s loop 2, in the presence of E3^{RanBP2}, and (ii) the Leu65–Arg70 region of SUMO, in the absence of E3^{RanBP2}.

Materials and Methods

Molecular dynamics simulations

To observe catalysis-related conformational changes, we simulated the step prior to the SUMO conjugation. The isopeptide bond between SUMO and Target^{RanGAP1} was broken and a new thioester bond between SUMO and E2^{Ubc9} was modeled. To observe the contribution of E3^{RanBP2}, two PDB files were generated. In the first, the structure was composed of the same monomers as in 1Z5S (with a modeled thioester bond between E2^{Ubc9} and SUMO); in the second file, E3^{RanBP2} was excluded from the complex (with a modeled thioester bond between E2^{Ubc9} and SUMO). We also carried out MD simulations for two monomers, E2^{Ubc9} (PDB ID: 1A5R)[32] and SUMO (PDB ID: 1A3S).[33] AMBER 8.0[34,35] was used for the simulations. The simulation time scales for each protein were 32.5 ns for E2^{Ubc9}, 50 ns for SUMO, 48.5 ns for E2^{Ubc9}–E3^{RanBP2}–SUMO–Target^{RanGAP1}, and 43 ns for E2^{Ubc9}–SUMO–Target^{RanGAP1}. The equilibration times were 2 ns for E2^{Ubc9}, 2.5 ns for SUMO, 2 ns for E2^{Ubc9}–E3^{RanBP2}–SUMO–Target^{RanGAP1}, and 5 ns for E2^{Ubc9}–SUMO–Target^{RanGAP1}. For the E2^{Ubc9}–E3^{RanBP2}–SUMO–Target^{RanGAP1} and E2^{Ubc9}–SUMO–Target^{RanGAP1} complexes, a second set of simulation was performed in order to validate the proposed allosteric mechanisms. The control set was 28 ns long for each complex, with equilibration times of 2.5 ns and 5 ns for E3^{RanBP2}–SUMO–Target^{RanGAP1} and E2^{Ubc9}–SUMO–Target^{RanGAP1}, respectively. In all trajectory analyses, equilibration times were excluded.

Author Manuscript Author Manuscript Author Manuscript Author Manuscript

Simulation parameters

The AMBER package[34,35] was used for the MD simulations. ff03 was the force field for all of simulations. Using the TIP3P water model,[36] the protein was solvated explicitly in a truncated octahedron box. Isobaric periodic boundary conditions were used with isotropic position scaling. The initial velocities of atoms were generated at 10 K with a Maxwellian distribution. The temperature was next gradually raised to 300 K; the system temperature was maintained at this temperature. The pressure was kept at 1 bar by the Berendsen weak-coupling approach.[37] In order to calculate the full electrostatic energy of a periodic box, the particle mesh Ewald method[38] with a cutoff distance of 9 Å was used. The constraints for the hydrogen bonds were set by the use of the SHAKE algorithm.[39] A time step of 2 fs was employed in the Leapfrog algorithm. Coordinates and energies were written every 1 ps.

Modeling of the thioester bond

We modeled a thioester bond between Cys93 of $E2^{Ubc9}$ and Gly97 of SUMO. For bond formation, the parameters were either taken from the classical parameters of AMBER or produced by using General Amber Force Field with the utilization of Antechamber program.[34,35] In forming the thioester bond, two distinct residue types, Glb and Cyx, were used instead of Gly and Cys. A new residue type, Glb, was defined by excluding the –COOH end of the Gly97. For Glb, the atom types, the point charges, and the parameters for van der Waals interactions of Gly were used. For the case of Cys, the atom types, the point charges, and the parameters for van der Waals interactions of an existing residue Cyx were used. Generally, Cyx was employed for the case of disulphide bond formation. In the crystal structure, the Glb and Cyx residues were not in an optimal orientation for the formation of the thioester bond. Thus, the Gaussian program was used for geometry optimization.[40–42] By utilizing the Gaussian method B3LYP/6–31+G**, the residues were oriented into a close geometry. In the generation of the stretching, bending, and torsional parameters of the new geometrical orientation, GAFF and Antechamber were used. By making use of these parameters, the thioester bond between Cyx93 and Glb97 was formed with the tleap program of the AMBER.

RMSD calculations

RMSD gives a measure for the MSF of the snapshots from the equilibrium state of the protein. We considered the first snapshot after the equilibration as the reference structure. After that, the distances between the C^{α} of the superimposed proteins were calculated. We used the ptraj module of AMBER 8.0[34,35] for calculating the MSF. For the RMSD calculation of SUMO, residues 1 to 19 were eliminated, since they are quite flexible and lie at the N-terminus of SUMO.

Clustering analysis

The clustering of the generated conformations was based on RMSD. This similarity measure represents the conformational difference between each pair of superimposed structures.[43] In the case of individual clustering, the conformations were superimposed on the average structure, calculated over the time course of the simulation of each case, assuming equilibrium fluctuations. For the case where the simulations were clustered together, the

Author Manuscript Author Manuscript Author Manuscript Author Manuscript

conformations were superimposed on the $E2^{Ubc9}$ taken at 15 ns of the $E2^{Ubc9}$–$E3^{RanBP2}$–SUMO–$Target^{RanGAP1}$ complex trajectory. The clustering was done via the MMTSB Toolset's[44] kclust utility, which utilizes *k*-means clustering. Within the RMSD threshold, the frames were divided into clusters and time windows based on their similarity measure. The RMSD threshold was set at 3 Å for joint clustering, 2.5 Å for the $E2^{Ubc9}$–$E3^{RanBP2}$–SUMO–$Target^{RanGAP1}$ complex, and 2.5 Å and 2.2 Å for $E2^{Ubc9}$–SUMO–$Target^{RanGAP1}$.

Calculation of the correlations between fluctuations

The normalized correlations between the mean-square fluctuations of atomic positions are defined as:

$$CO_{i,j} = \frac{\langle \Delta R_i \Delta R_j \rangle}{\langle \Delta R_i^2 \rangle^{1/2} \langle \Delta R_j^2 \rangle^{1/2}} \quad (1)$$

In Eq. (1), ΔR_i is the fluctuation of the position vector R_i; ΔR_j is the fluctuation of the position vector R_j. i and j stand for the residues of interest. The brackets represent ensemble averages over calculated snapshots. The cross-correlations range in the interval of [−1, 1]. −1 designates fully anti-correlated and 1 designates fully correlated atomic fluctuations. The normalized correlations between the mean square fluctuations were calculated within the time windows defined by the clustering analysis.

Supplementary Material

Refer to Web version on PubMed Central for supplementary material.

Acknowledgements

This project was funded in whole or in part with federal funds from the National Cancer Institute, National Institutes of Health, under contract no. HHSN261200800001E. This research was supported in part by the Intramural Research Program of the National Institutes of Health, National Cancer Institute, Center for Cancer Research. The content of this publication does not necessarily reflect the views or policies of the Department of Health and Human Services, nor does mention of trade names, commercial products, or organizations imply endorsement by the U.S. Government. R.L. acknowledges support from the NIH extramural program. T. H. acknowledges support from the Betil Fund, TUBA (Turkish Academy of Sciences), DPT (2009K120520), and TUBITAK project (TUBITAK, 107T382). The authors thank Bulent Balta for helpful discussions and Seren Soner for technical support.

Abbreviations used:

MSF	mean-square fluctuations
SUMO	small ubiquitin-like modifier
Ubl	ubiquitin
SIM	SUMO interaction motif

Author Manuscript Author Manuscript Author Manuscript Author Manuscript

References

1. Mo YY, Yu YN, Theodosiou E, Ee PLR &Beck WT (2005). A role for Ubc9 in tumorigenesis. Oncogene, 24, 2677–2683. [PubMed: 15735760]
2. Zhao J. (2007). Sumoylation regulates diverse biological processes. Cell. Mol. Life Sci 64, 3017–3033. [PubMed: 17763827]
3. Melchior F. (2000). Sumo—nonclassical ubiquitin. Annu. Rev. Cell Dev. Biol 16, 591–626. [PubMed: 11031248]
4. Seeler JS & Dejean A. (2003). Nuclear and unclear-functions of SUMO. Nat. Rev. Mol. Cell Biol 4, 690–699. [PubMed: 14506472]
5. Martin S, Wilkinson KA, Nishimune A. & Henley JM (2007). Emerging extranuclear roles of protein SUMOylation in neuronal function and dysfunction. Nat. Rev. Neurosci 8, 948–959. [PubMed: 17987030]
6. Baek SH (2006). A novel link between SUMO modification and cancer metastasis. Cell Cycle, 5, 1492–1495. [PubMed: 16861889]
7. Boggio R. & Chiocca S. (2006). Viruses and sumoylation: recent highlights. Curr. Opin. Microbiol 9, 430–436. [PubMed: 16815735]
8. Hochstrasser M. (2002). New structural clues to substrate specificity in the “ubiquitin system.” Mol. Cell, 9, 453–454. [PubMed: 11931752]
9. Nalepa G, Rolfe M. & Harper JW (2006). Drug discovery in the ubiquitin–proteasome system. Nat. Rev. Drug Discovery, 5, 596–613. [PubMed: 16816840]
10. Kirkin V. & Dikic I. (2007). Role of ubiquitin- and Ubl-binding proteins in cell signaling. Curr. Opin. Cell Biol 19, 199–205. [PubMed: 17303403]
11. Watson IR & Irwin MS (2006). Ubiquitin and ubiquitin-like modifications of the p53 family. Neoplasia, 8, 655–666. [PubMed: 16925948]
12. Hoeller D, Hecker CM & Dikic I. (2006). Ubiquitin and ubiquitin-like proteins in cancer pathogenesis. Nat. Rev. Cancer, 6, 776–788. [PubMed: 16990855]
13. Dye BT & Schulman BA (2007). Structural mechanisms underlying posttranslational modification by ubiquitin-like proteins. Annu. Rev. Biophys. Biomol. Struct 36, 131–150. [PubMed: 17477837]
14. Capili AD & Lima CD (2007). Taking it step by step: mechanistic insights from structural studies of ubiquitin/ubiquitin-like protein modification pathways. Curr. Opin. Struct. Biol 17, 726–735. [PubMed: 17919899]
15. Reverter D. & Lima CD (2005). Insights into E3 ligase activity revealed by a SUMO-RanGAP1–Ubc9–Nup358 complex. Nature, 435, 687–692. [PubMed: 15931224]
16. Tatham MH, Chen Y. & Hay RT (2003). Role of two residues proximal to the active site of Ubc9 in substrate recognition by the Ubc9 center dot SUMO-1 thiolester complex. Biochemistry, 42, 3168–3179. [PubMed: 12641448]
17. Bernier-Villamor V, Sampson DA, Matunis MJ &Lima CD (2002). Structural basis for E2-mediated SUMO conjugation revealed by a complex between ubiquitin-conjugating enzyme Ubc9 and RanGAP1. Cell, 108, 345–356. [PubMed: 11853669]
18. Duda DM & Schulman BA (2005). Tag-team SUMO wrestling. Mol. Cell, 18, 612–614. [PubMed: 15949435]
19. Heun P. (2007). SUMOrganization of the nucleus. Curr. Opin. Cell Biol, 19, 350–355. [PubMed: 17467254]
20. Geiss-Friedlander R. & Melchior F. (2007). Concepts in sumoylation: a decade on. Nat. Rev. Mol. Cell Biol 8, 947–956. [PubMed: 18000527]
21. Johnson ES (2004). Protein modification by SUMO. Annu. Rev. Biochem 73, 355–382. [PubMed: 15189146]
22. Pichler A, Knipscheer P, Saitoh H, Sixma TK &Melchior F. (2004). The RanBP2 SUMO E3 ligase is neither HECT- nor RING-type. Nat. Struct. Mol. Biol 11, 984–991. [PubMed: 15378033]
23. Muller S, Hoege C, Pyrowolakis G. & Jentsch S. (2001). Sumo, ubiquitin’s mysterious cousin. Nat. Rev. Mol. Cell Biol 2, 202–210. [PubMed: 11265250]

Author Manuscript Author Manuscript Author Manuscript Author Manuscript

24. Macauley MS, Errington WJ, Okon M, Scharpf M, Mackereth CD, Schulman BA & McIntosh LP (2004). Structural and dynamic independence of isopeptide-linked RanGAP1 and SUMO-1. J. Biol. Chem 279, 49131–49137. [PubMed: 15355965]
25. Tatham MH, Kim S, Jaffray E, Song J, Chen Y. &Hay RT (2005). Unique binding interactions among Ubc9, SUMO and RanBP2 reveal a mechanism for SUMO paralog selection. Nat. Struct. Mol. Biol 12, 67–74. [PubMed: 15608651]
26. Tang ZS, Hecker CM, Scheschonka A. & Betz H. (2008). Protein interactions in the sumoylation cascade—lessons from X-ray structures. FEBS J. 275, 3003–3015. [PubMed: 18492068]
27. Zhu SS, Goeres J, Sixt KM, Bekes M, Zhang XD, Salvesen GS & Matunis MJ (2009). Protection from isopeptidase-mediated deconjugation regulates paralog-selective sumoylation of RanGAP1. Mol. Cell, 33, 570–580. [PubMed: 19285941]
28. Matunis MJ & Pickart CM (2005). Beginning at the end with SUMO. Nat. Struct. Mol. Biol 12, 565–566. [PubMed: 15999109]
29. Song J, Durrin LK, Wilkinson TA, Krontiris TG& Chen YA (2004). Identification of a SUMO-binding motif that recognizes SUMO-modified proteins. Proc. Natl Acad. Sci. USA, 101, 14373–14378. [PubMed: 15388847]
30. Tozluoğlu M, Karaca E, Nussinov R. & Haliloğlu T. (in press). A mechanistic view of the role of E3 in sumoylation. PLoS Comput. Biol 6, e1000913.
31. Armon A, Graur D. & Ben-Tal N. (2001). ConSurf: an algorithmic tool for the identification of functional regions in proteins by surface mapping of phylogenetic information. J. Mol. Biol 307, 447–463. [PubMed: 11243830]
32. Bayer P, Arndt A, Metzger S, Mahajan R, Melchior F, Jaenicke R. & Becker J. (1998). Structure determination of the small ubiquitin-related modifier SUMO-1. J. Mol. Biol 280, 275–286. [PubMed: 9654451]
33. Giraud MF, Desterro JMP & Naismith JH(1998). Structure of ubiquitin-conjugating enzyme 9 displays significant differences with other ubiquitin-conjugating enzymes which may reflect its specificity for sumo rather than ubiquitin. Acta Crystallogr., Sect. D: Biol. Crystallogr 54, 891–898. [PubMed: 9757105]
34. Case DA, Darden TA III, Simmerling TEC, Wang CL, Duke J, E R. et al. (2004). AMBER 8, p. 310, University of California, San Francisco.
35. Case DA, Cheatham TE, Darden T, Gohlke H, Luo R, Merz KM et al. (2005). The Amber biomolecular simulation programs. J. Comput. Chem 26, 1668–1688. [PubMed: 16200636]
36. Jorgensen WL, Chandrasekhar J, Madura JD, Impey RW & Klein ML (1983). Comparison of simple potential functions for simulating liquid water. J. Chem. Phys 79, 926–935.
37. Berendsen HJC, Postma JPM, Vangunsteren WF, Dinola A. & Haak JR (1984). Molecular-dynamics with coupling to an external bath. J. Chem. Phys 81, 3684–3690.
38. Essmann U, Perera L, Berkowitz ML, Darden T, Lee H. & Pedersen LG (1995). A smooth particle mesh Ewald method. J. Chem. Phys 103, 8577–8593.
39. Ryckaert JP, Ciccotti G. & Berendsen HJC(1977). Numerical-integration of cartesian equations of motion of a system with constraints—molecular-dynamics of N-alkanes. J. Comput. Phys 23, 327–341.
40. Becke AD (1993). A new mixing of Hartree-Fock and local density-functional theories. J. Chem. Phys 98, 1372–1377.
41. Becke AD (1993). Density-functional thermochemistry. 3. The role of exact exchange. J. Chem. Phys 98, 5648–5652.
42. Becke AD (1988). Density-functional exchange-energy approximation with correct asymptotic-behavior. Phys. Rev. A, 38, 3098–3100.
43. Leach A. (2001). Molecular Modelling: Principles and Applications. 2 edit. Prentice Hall.
44. Feig M, Karanicolas J. & Brooks CL (2004). MMTSB Tool Set: enhanced sampling and multiscale modeling methods for applications in structural biology. J. Mol. Graphics Modell 22, 377–395.

Author Manuscript Author Manuscript Author Manuscript Author Manuscript

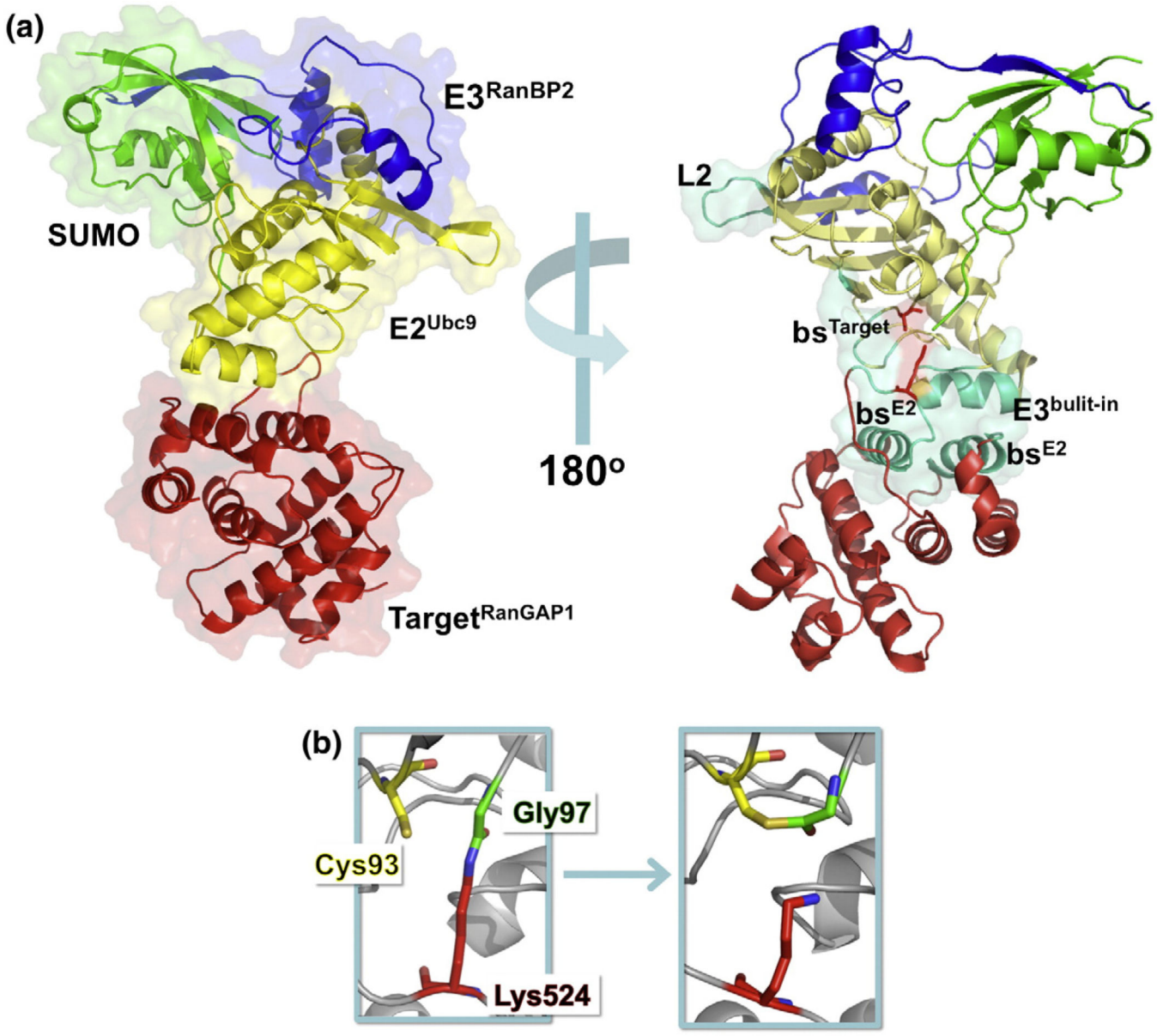

Fig. 1.

(a) Stereo view of the $E2^{Ubc9}$–$E3^{RanBP2}$–SUMO–$Target^{RanGAP1}$ complex (PDB ID: 1Z5S). $E2^{Ubc9}$ is colored yellow, $E3^{RanBP2}$ is in blue, SUMO is in green, and $Target^{RanGAP1}$ in red. Left: Each protein is labeled and shown in cartoon and transparent surface representation. Right: The functional and structural important regions are colored in green-cyan and are represented in cartoon and transparent surface. The depicted regions of $E2^{Ubc9}$ are loop 2 (L2), Target binding site (bs^{Target}), catalytic residue ($E2^{catalytic}$), and inherent E3 region of $E2^{Ubc9}$ ($E3^{built\text{-}in}$). For $Target^{RanGAP1}$, $E2^{Ubc9}$ binding sites (bs^{E2}) and its catalytic residue ($Target^{catalytic}$) are highlighted. The catalytic residues of both $E2^{Ubc9}$ (Cys93) and $Target^{RanGAP1}$ (Lys524) are shown as stick representations (red). (b) Modeling of the thioester bond. In the crystal structure of the $E2^{Ubc9}$–$E3^{RanBP2}$–SUMO–$Target^{RanGAP1}$ complex, the C-terminal tail of SUMO (Gly97) is attached to the catalytic lysine (Lys524) of

Author Manuscript Author Manuscript Author Manuscript Author Manuscript

Target^{RanGAP1} via an isopeptide bond. In order to observe the sequence of events that lead the system to catalysis, this isopeptide bond is broken and a new thioester bond is modeled between E2^{Ubc9} (Cys93) and SUMO (Gly97).

Author Manuscript Author Manuscript Author Manuscript Author Manuscript

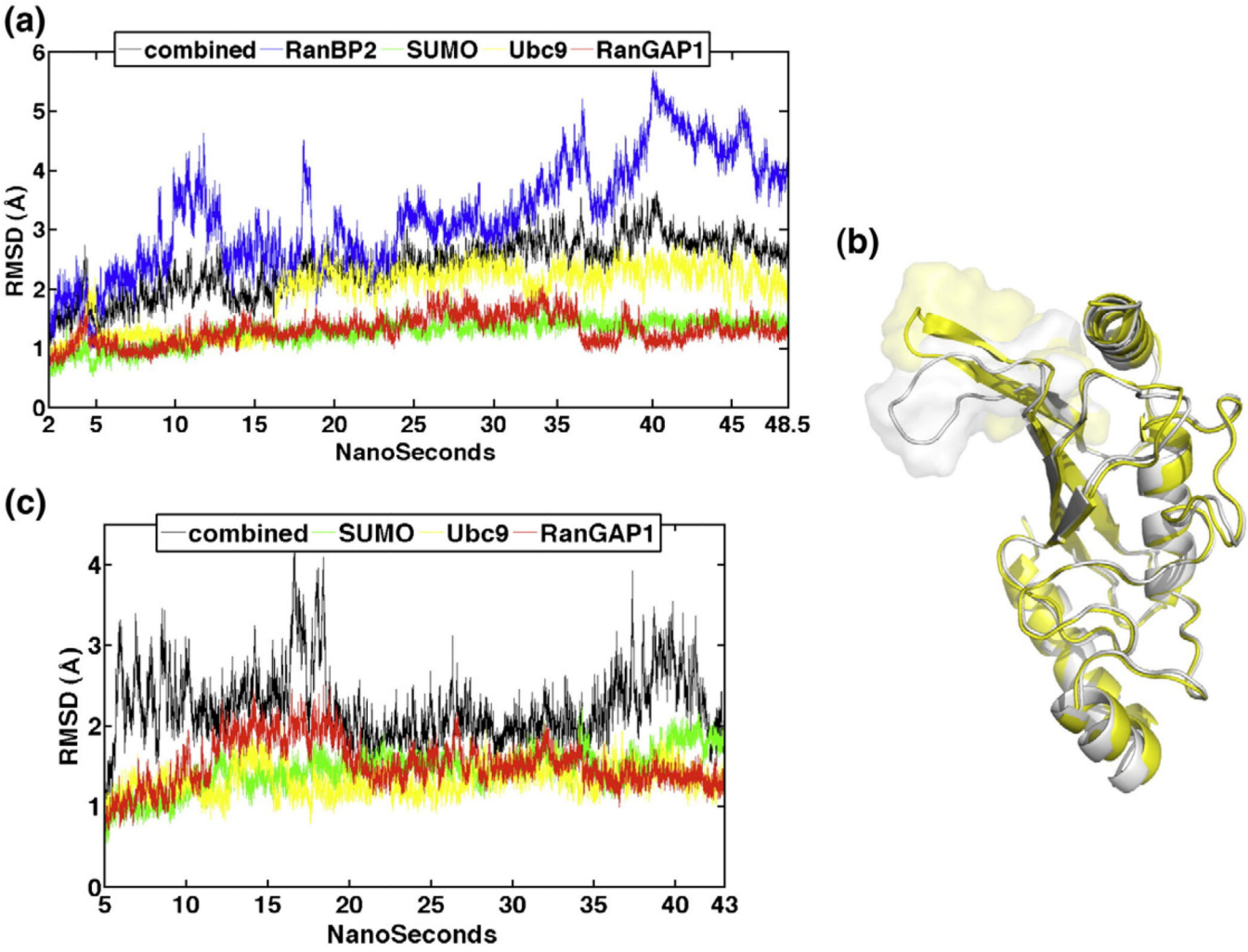

Fig. 2.

(a) RMSD evaluation of the $E2^{Ubc9}$–$E3^{RanBP2}$–SUMO–$Target^{RanGAP1}$ complex over the time course of the simulation of 48.5 ns. The color code of each line is indicated in the legend. (b) Extent of the conformational change observed in loop 2 of $E2^{Ubc9}$. Loop 2 is represented in transparent surface and cartoon and the rest of $E2^{Ubc9}$ is shown in cartoon. The white snapshot is extracted from 10 ns and the yellow one from 24 ns. (c) RMSD evaluation of the $E2^{Ubc9}$–SUMO–$Target^{RanGAP1}$ complex over the time course of the simulation of 43 ns. The color code of each line is indicated in the legend.

Author Manuscript Author Manuscript Author Manuscript Author Manuscript

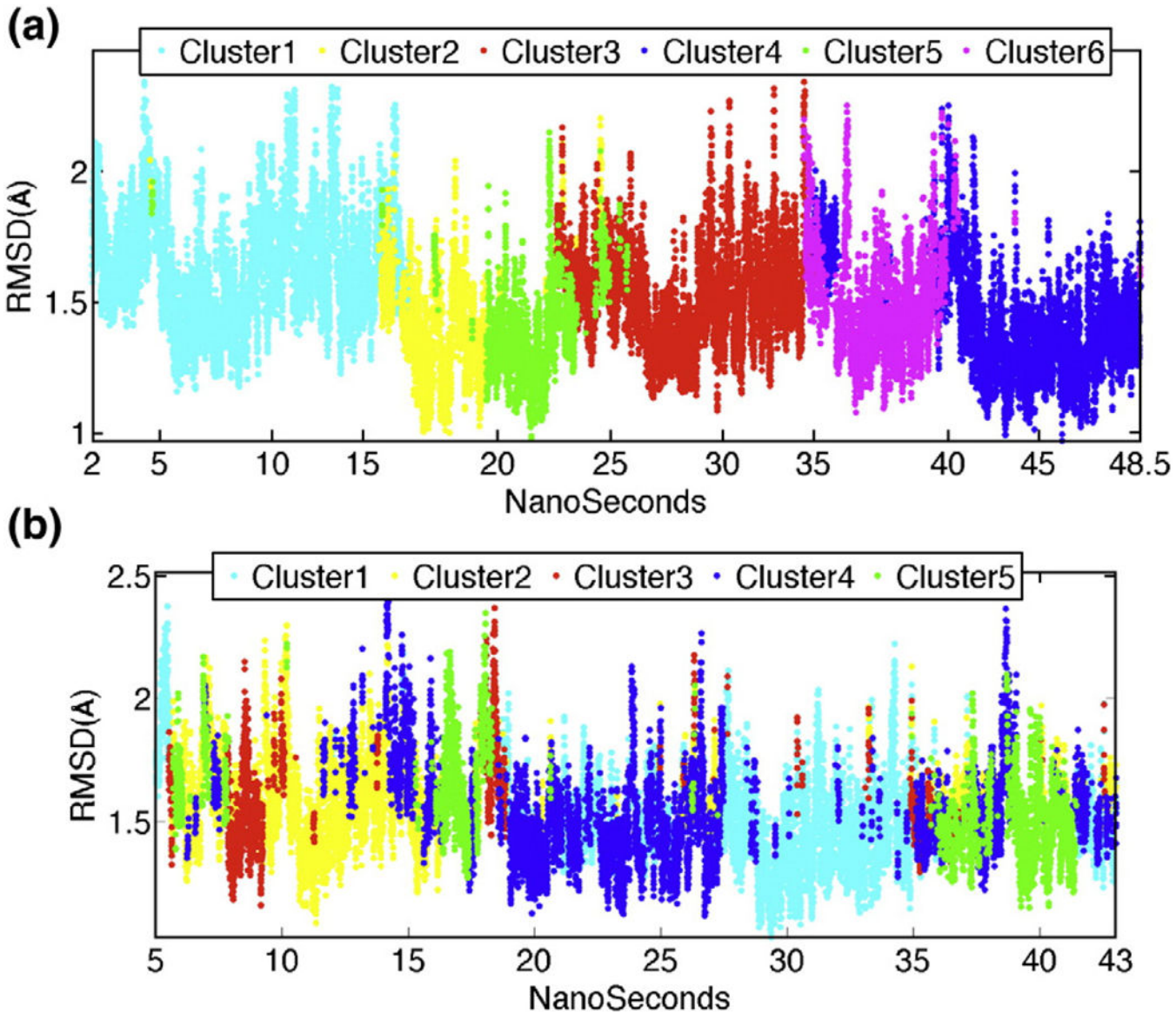

Fig. 3.

(a) RMSD evaluation of the $E2^{Ubc9}$–$E3^{RanBP2}$–SUMO–$Target^{RanGAP1}$ complex after clustering with an RMSD threshold of 2.5 Å over the time course of the simulation of 48.5 ns. The color code of each line represents a different conformational ensemble. (b) RMSD evaluation of the $E2^{Ubc9}$–SUMO–$Target^{RanGAP1}$ complex after clustering with an RMSD threshold of 2.5 Å over the time course of the simulation of 43 ns. The color code of each line represents a different conformational ensemble.

Author Manuscript Author Manuscript Author Manuscript Author Manuscript

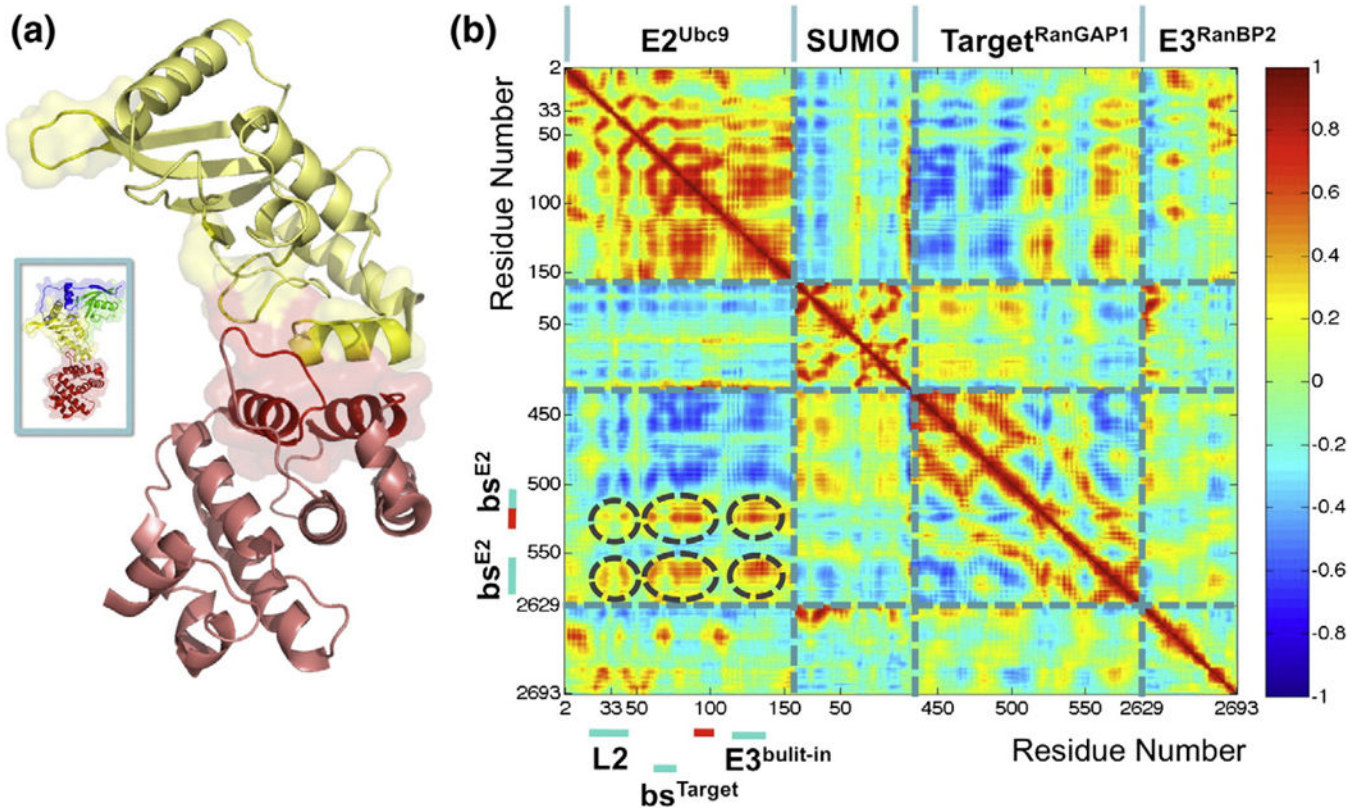

Fig. 4.

(a) Regions of the $E2^{Ubc9}$–$Target^{RanGAP1}$ complex that show coupled correlated fluctuations. The monomer positions of the illustrated $E2^{Ubc9}$ (yellow)–$Target^{RanGAP1}$ (dark red) complex are extracted from the PDB entry 1Z5S. The cartoon and transparent surface represented regions correspond to the encircled correlations on the left panel. The spatial arrangement of the $E2^{Ubc9}$–$Target^{RanGAP1}$ complex in the overall configuration of the $E2^{Ubc9}$–$E3^{RanBP2}$–SUMO–$Target^{RanGAP1}$ complex is shown in the box on the left. (b) The coupled correlated fluctuations observed for the $E2^{Ubc9}$–$E3^{RanBP2}$–SUMO–$Target^{RanGAP1}$ complex imply an allosteric effect. The correlation plot is derived from the $E2^{Ubc9}$–$E3^{RanBP2}$–SUMO–$Target^{RanGAP1}$ complex trajectory within the time interval of 2–15 ns. The coloring scheme is the same as in Fig. 2a.In the plot, the important correlations are encircled in dark grey. Where these encircled regions correspond to on $E2^{Ubc9}$ and $Target^{RanGAP1}$ are also highlighted next to the axes. The highly correlated regions spotted in circles show that the loop 2 of $E2^{Ubc9}$ moves in accordance with the functional and structural important regions of the $E2^{Ubc9}$–$Target^{RanGAP1}$ complex.

Author Manuscript
Author Manuscript
Author Manuscript
Author Manuscript

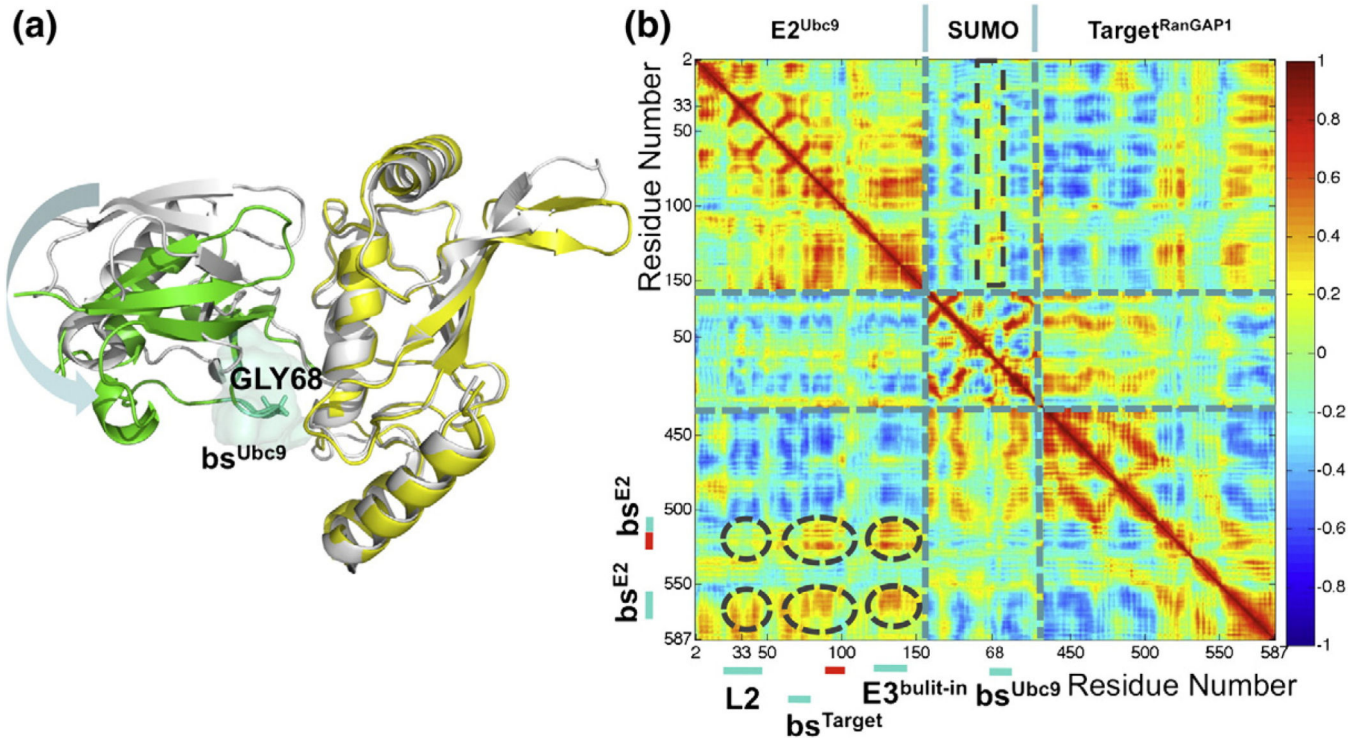

Fig. 5.

(a) The lack of $E3^{RanBP2}$ leads to the formation of a new interaction surface in the $E2^{Ubc9}$–SUMO complex. The $E2^{Ubc9}$–SUMO complex taken from the crystal structure of the $E2^{Ubc9}$–$E3^{RanBP2}$–SUMO–$Target^{RanGAP1}$ is shown in light grey. The colored monomers ($E2^{Ubc9}$ in yellow and SUMO in green) belong to the snapshot taken from the $E2^{Ubc9}$–SUMO–$Target^{RanGAP1}$ trajectory at 19.3 ns. The absence of E3 leads to an orientational change in SUMO, which results in the formation of a new binding interface between SUMO and $E2^{Ubc9}$. The interaction surface on SUMO side (bs^{Ubc9}) is colored in green-cyan and shown in ribbon and transparent surface. Gly68 residue is shown explicitly, since among the newly formed interfaces, it has the tightest contact with $E2^{Ubc9}$. (b) The new $E2^{Ubc9}$–SUMO interface formed upon removal of $E3^{RanBP2}$ indicates correlated fluctuations with $E2^{Ubc9}$'s loop 2. This correlation plot is calculated from the trajectory of the $E2^{Ubc9}$–SUMO–$Target^{RanGAP1}$ complex. The time interval taken in to account is 18–25 ns. The newly formed $E2^{Ubc9}$–SUMO interface changes the network of correlations in the rest of the protein (The most important regions are encircled). The correlation plot reveals that the core of the new interface on the SUMO side is anti-correlated with $E2^{Ubc9}$'s loop 2. This observation indicates that a new path is added in the sequence of events upon removal of $E3^{RanBP2}$.

Author Manuscript

Author Manuscript

Author Manuscript

Author Manuscript

Table 1.

Various RMSD values for the $E2^{Ubc9}$–$E3^{RanBP2}$–SUMO–$Target^{RanGAP1}$ and $E2^{Ubc9}$–SUMO–$Target^{RanGAP1}$ complex trajectories

	$E2^{Ubc9}$–$E3^{RanBP2}$–SUMO–$Target^{RanGAP1}$	$E2^{Ubc9}$–SUMO–$Target^{RanGAP1}$
Overall RMSD (Å)	2.4±0.5 (3.6–0.6)[a]	2.2±0.4 (4.2–0.6)
	2.1±0.4 (3.3–0.6)[b]	
Individual chain-based RMSD (Å)		
SUMO	1.3±0.2 (1.9–0.5)	1.5±0.2 (2.2–0.5)
$E2^{Ubc9}$	1.9±0.5 (2.8–0.5)	1.3±0.2 (2.1–0.6)
$Target^{RanGAP1}$	1.3±0.2 (2.0–0.6)	1.5±0.3 (2.5–0.5)
$E3^{RanBP2}$	3.2±0.9 (5.7–0.6)	—

Each entry corresponds to mean±SD of the RMSD values. The maximum and minimum values of the data set are indicated in parentheses.

[a] The RMSD is calculated over the trajectory of $E2^{Ubc9}$–$E3^{RanBP2}$–SUMO–$Target^{RanGAP1}$.

[b] Before calculating the RMSD of the $E2^{Ubc9}$–$E3^{RanBP2}$–SUMO–$Target^{RanGAP1}$ complex, $E3^{RanBP2}$ is extracted from the system. Thus, the reported results are calculated over three monomers: $E2^{Ubc9}$–SUMO–$Target^{RanGAP1}$.

Author Manuscript Author Manuscript Author Manuscript Author Manuscript

Table 2.

Indication of $E2^{Ubc9}$'s important atomic positional fluctuation values (in angstrom)[a]

	Isolated $E2^{Ubc9}$	**$E2^{Ubc9}$–$E3^{RanBP2}$–SUMO–$Target^{RanGAP1}$**	**$E2^{Ubc9}$–SUMO–$Target^{RanGAP1}$**
For the whole simulation time			
$E2^{Ubc9}$'s loop 2	3.7±1.9	19.9±13.6	8.6±4.9
The whole protein except loop 2	0.7±0.7	0.6±0.6	0.6±0.6
$E2^{Ubc9}$'s catalytic Cys	1.8	0.3	0.2
$E2^{Ubc9}$'s built-in E3	1.1±0.2	0.8±0.3	0.6±0.3
For specific time periods of $E2^{Ubc9}$–$E3^{RanBP2}$–SUMO–$Target^{RanGAP1}$			
	2–15 ns	19–24 ns	25–30 ns[b]
$E2^{Ubc9}$'s loop 2	4.5±2.8	4.5±2.8	4.1±2.3
$E3^{RanBP2}$'s flexible linker (Asp2665–Asp2673)	6.3±4.1	5.0±4.2	3.1±1.5
For specific time periods of $E2^{Ubc9}$–SUMO–$Target^{RanGAP1}$			
	5.5–7.5 ns[b]	17–25 ns	
$E2^{Ubc9}$'s loop 2	1.6±0.4	3.0±2.2	

[a] Each entry corresponds to mean±SD of the atomic positional fluctuation values. The maximum and minimum values of the data set are indicated in parentheses.

[b] The time intervals are selected from the time windows where no strong correlation is observed at the $E2^{Ubc9}$–$Target^{RanGAP1}$ interface.

Author Manuscript

Author Manuscript

Author Manuscript

Author Manuscript

Table 3.

The distribution of the conformations revealed by joint clustering

	$E2^{Ubc9}$–$E3^{RanBP2}$–SUMO–$Target^{RanGAP1}$	**$E2^{Ubc9}$–SUMO–$Target^{RanGAP1}$**
$E2^{Ubc9}$–SUMO–$Target^{RanGAP1}$		
Ensemble 1	100	0
Ensemble 2	0	71.5
Ensemble 3	0	28.2
Total	100	100
$E2^{Ubc9}$		
Ensemble 1	73.3	99.1
Ensemble 2	26.7	0.9
Total	100	100

The values indicated are in percentage.